5

Liver Segmentation and Volume Estimation from Preoperative CT Images in Hepatic Surgical Planning: Application of a Semiautomatic Method Based on 3D Level Sets

Laura Fernandez-de-Manuel[1,5], Maria J. Ledesma-Carbayo[1,5], Daniel Jimenez-Carretero[1,5], Javier Pascau[2], Jose L. Rubio-Guivernau[1,5], Jose M. Tellado[3], Enrique Ramon[4], Manuel Desco[2] and Andres Santos[1,5]

[1]*Biomedical Image Technologies Lab, Universidad Politécnica de Madrid*
[2]*Medicina y Cirugía Experimental, Hospital General Universitario Gregorio Marañón*
[3] *Servicio de Cirugía General I, Hospital General Universitario Gregorio Marañón*
[4] *Servicio de Radiodiagnóstico, Hospital General Universitario Gregorio Marañón, Madrid*
[5]*Biomedical Research Center in Bioengineering, Biomaterials, and Nanomedicine (CIBER-BBN), Madrid*
Spain

1. Introduction

The advances in the understanding of the liver anatomy and physiology (Couinaud, 1999; Ryu & Cho, 2009), the improvement of medical imaging techniques (Radtke et al., 2007; Handels & Ehrhardt, 2009) and the progressive security of surgical instrumentation, allow surgeons to design complex liver resections more accurately and efficacious without jeopardizing patient safety. Pre-operative planning has become an essential task before undertake liver surgery, and requires mandatory mapping of both inflow and outflow hepatic vasculature, the assessment of the number and spatial relationships of the tumor(s), and frequently, an estimation of the future remnant liver volume (FRLV). Several determinants may modify threshold levels for a safe FRLV (for example, the presence and extension of cirrhosis, esteatosis or post-chemotherapy sinusoidal obstructive syndrome). Therefore, healthy functional liver volume estimation and functional performance analysis are tests further needed to make the final clinical decision before extensive hepatectomies.
Traditionally, FRLV has been extrapolated from preoperative computed tomography (CT) images using hepatic segmentation done manually in an otherwise time and labour-consuming process. Briefly, some commercial systems include tools that allow radiologists to manually segment 2D slices of a CT study in transverse (axial) views. Due to the high number of slices (usually ranging from 100 to 500 depending on the scanner), a sub-sampled version of the original CT is used in daily planning. However, even when using a sub-sampled version, the complete procedure takes longer than 30 minutes.

Many research groups work nowadays in the development of automatic and semiautomatic liver segmentation tools in order to help clinicians saving time and effort and increasing precision. Since the liver is located adjacent to other organs of similar CT gray values, and it presents a huge variability in size and shape among different patients, the development of segmentation tools has become a challenging problem with increasing interest in the last few years.

In this work we first present a summary of the state of the art in this field. Secondly, we propose the application of a semiautomatic tool to segment the healthy part of the liver and estimate the healthy liver volume from CT preoperative abdominal images, using techniques based on a sophisticated 3D Level Sets definition (Fernandez-de-Manuel et al., 2009) that combines intensity, gradient information and curvature restrictions extended with a morphological image pre-processing and a method to easily define 3D frontiers with adjacent regions. The algorithm has been developed to solve a specific request demanded by radiologists from the research team. The requirement in our work is that the segmentation should include only healthy parenchyma excluding tumors in order not to overestimate healthy liver volumes.

The proposed tool has been validated with several preoperative CT abdominal data sets. Resulting segmentations have been evaluated with respect to those obtained from radiologists' manual segmentations and supervised by clinicians.

2. State of the art

As it has been briefly introduced, the development of automatic and semiautomatic liver segmentation tools is particularly challenging due to liver's variability in size and shape and to the proximity to other organs of similar intensity values which generates blurred edges in CT images. Many works have been published in this field.

First attempts to perform automatic liver segmentation were based on gray-level statistics (Woodhouse et al., 1994; Gao et al., 1996). Liver gray levels can be estimated either by statistical analysis of manually segmented slices, either by histogram analysis with the aim of establishing an a priori knowledge about liver density. In most of the works based on gray-level statistics, a threshold is used to generate a binary volume that is later processed by morphological operators in order to separate desired organs. Recent gray-level methods have been presented by Soler et al. (Soler et al., 2001), Fujimoto et al. (Fujimoto et al., 2002), Liu et al. (Liu et al., 2005) and Lim et al. (Lim et al., 2004; Lim et al., 2005; Lim et al., 2006). However, the high variability among liver CT images due to the differences of intensity values in different kind of tumors and the different settings regarding contrast media, make difficult the optimal operation of the methods just based on gray-level statistics. Other approaches try to overcome the problem of liver's gray-level estimation by learning gray-level features corresponding to the liver from different CT images with methods based on neural networks. Tsai and Tanahashi (Tsai & Tanahashi, 1994) , Koss et al. (Koss et al., 1999) and Lee et al. (Lee & Chung, 2000; Lee et al., 2003) presented examples of automatic detection and labeling of abdominal organs with neural networks. A common difficulty of this kind of methods is that they usually need a big and highly varied training set to learn the variability among different patients.

Liver segmentation based on anatomical knowledge regarding size, position and shape of each abdominal organ includes several works that employ statistical shape models (SSM) and shape constrained deformable models. Montagnat and Delingette (Montagnat &

Delingette, 1997), Gao et al. (Gao et al., 1998) and Lamecker et al. (Lamecker et al., 2004) presented several of these techniques. The drawback of these methods is the model construction, which requires a huge quantity of training data properly collected in order to capture all the possible shapes; a really challenging task regarding the high amount of variable and complex liver shapes and sizes. Besides, these algorithms use to fail when processing not standard liver shapes and require too much computation time to achieve a good matching between model and image. Other works are based on the construction of probabilistic atlases. That is the case of the works presented in (Park et al., 2003; Zhou et al., 2005; Shimizu et al., 2006). First, a registration step of training CT images into a standard space defined by landmarks (manually or automatically chosen) is needed. The probabilistic atlas is generated by spatially averaging the registered surfaces. Then, it is used to compute the probability of belonging to a certain organ for each voxel in the image. Finally, the region that maximizes the posterior probability of being the desired organ is extracted by thresholding or using an iterative algorithm. This type of techniques carries several problems. Firstly, the huge amount of training images required. Secondly, the difficulty of finding an appropriate probability function. Finally, the high computation times required.

Some variants of region growing have been also applied to liver segmentation (Pohle & Toennies, 2001; Ruskó et al., 2007). However, for those cases, sophisticated restriction methods have to be taken into account in order to avoid over-flooding.

Live wire algorithms (Barrett & Mortensen, 1997) are the basis of several semiautomatic liver volume extraction tools currently used in clinical practice. An image is described as an undirected and weighted graph where pixels are represented by the vertexes, the edges connect neighboring pixels, and their weighs represent the cost of the connections computed from image features like gray value, gradient magnitude, gradient direction or Laplacian zero-crossing among others. Dijkstra's graph-search algorithm computes all possible minimum-cost paths between a starting seed point established by the user on the liver boundary and all the possible points in the image. After that, a desired boundary can be interactively chosen by selecting a free point with the mouse. Indeed, when the mouse pointer moves over the image, the previous boundary segment is deleted and the new minimal path between the seed point and the new position is displayed. When that minimal path is close to the desired boundary, the user can freeze it by adding a new seed point. It causes the reinitialization of the boundary detection. Thus, this process allows the user to have a full control over the segmentation. Many variants of this technique have been developed for years. In (Schenk et al., 2000; Schenk et al., 2001) the authors modified the original algorithm to reduce its computation time in order to extend it to 3D images. These methods speed up the work of radiologists manually drawing liver boundaries, but are highly dependent on the operator's skill.

Different approaches widely used in liver segmentation are Level Sets and snakes (Caselles et al., 1997; Pan & Dawant, 2001; Bekes et al., 2007; Garamendi et al., 2007; Lee et al., 2007; Platero et al., 2008), based on a speed function that controls the front propagation of an implicitly defined surface toward the liver boundary. Moreover, the propagation may be constrained by an a priori anatomic information or shape restrictions. The main problem of Level Sets is the definition of an appropriate speed function and its parameters.

Finding an efficient liver segmentation algorithm able to provide good segmentation results from CT liver images and avoiding the classical problems of standard segmentation methods (such as over-flooding, under or over-segmentation, long computing times and so on) is such a challenging and important task that a recent competition has faced this

purpose. In October 2007, a contest whose aim was to compare different algorithms to segment the liver from clinical 3D CT scans was hold as part of the workshop *3D Segmentation in the Clinic: A Grand Challenge* in conjunction with MICCAI 2007 (Van Ginneken et al., 2007; Heimann et al., 2009). Teams that participated in the liver segmentation contest downloaded training and test data and submitted the results of their algorithms on test data both before and during the workshop. To evaluate the quality of a given segmentation, segmentations were compared to expert-generated references and rated according to detected deviations: Volumetric Overlap Error, Relative Volume Difference, Average Symmetric Surface Distance, Root Mean Square Symmetric Surface Distance and Maximum Symmetric Surface Distance. Some of the most successful proposals that got better punctuation were automatic methods based on statistical shape models with some additional free deformation (Heimann et al., 2007; Kainmueller et al., 2007; Saddi et al., 2007) and interactive segmentation methods requiring certain amount of user interaction such as manual refinement after a graph cut or a region growing method (Beck & Aurich, 2007; Beichel et al., 2007), two dimensional Level Sets with initialization (Dawant et al., 2007; Lee et al., 2007) and three dimensional Level Sets with initialization of 2D contours (Wimmer et al., 2007). However, in that workshop, the segmentation was defined as the entire liver tissue including all internal structures like big vessels systems, tumors, etc. Therefore, that segmentation definition does not exactly match the actual goal of our work (that is estimating healthy liver volumes).

Recently, most of new liver segmentation methods combine different techniques: statistical shape models, mathematical morphology and Level Set approaches. (Linguraru et al., 2010) present a clinical tool developed to segment liver and spleen based on probabilistic atlases. The atlases are created using manually segmented data from non contrast CT images. The organ locations are modeled in the physical space and normalized to the position of the xiphoid. The construction of the atlases enables the automated quantifications of liver and spleen volumes and heights, later improved by a geodesic active contour. In (Suzuki et al., 2010) a computerized liver extraction scheme based on geodesic active contour segmentation combined with level-set contour evolution and applied to liver donor images is presented. In (Jiang & Cheng, 2009) a threshold segmentation is combined with morphological image processing and active contour models in order to extract the initial contour and segment the liver slice by slice. In (Campadelli et al., 2010) a fully automatic, gray-level based segmentation framework based on a multiplanar fast marching method is proposed. Other sophisticated methods are based on Support Vector Machines (Luo et al., 2009).

3. Proposed method

In this work we propose the application of a tool based on Level Sets to segment the healthy part of the liver in CT preoperative abdominal images. The tool has been developed following the requirements demanded by radiologists inside the team: segmentation of healthy parenchyma excluding tumors in order not to overestimate healthy liver volumes. In this sense the proposed function allows to directly segment healthy parenchyma.

The tool combines a 3D active contour algorithm previously introduced in (Fernandez-de-Manuel et al., 2009) with morphological filtering and a fast manual frontier definition, in order to estimate healthy liver volumes. SSM models have been discarded due to the aim of segmenting a wide variety of shapes, sizes and liver pathologies with different kind of

tumors and surgical stages. For this reason, a solution based on active contours with no "a prioris" has been approached. The proposed technique only requires the user to initialize a seed and different frontier points in the most common problematic regions before the automatic computation stage. In case that the first segmentation was not satisfactory, the user could redefine or add some other frontiers and repeat the automatic stage. Normally, the initial seed or frontiers do not need to be changed. Nevertheless, in clinical environment it is useful to give the opportunity to the radiologist of certain interaction that allows refining the segmentation having into account previous result. This is very useful in difficult and strange cases.

The proposed method has been validated with 5 preoperative CT abdominal data sets. Resulting segmentations have been numerically evaluated in terms of Overlap Error, Relative Volume Difference and Surface Distances with respect to radiologists' reference manual segmentations. The method has demonstrated good performance.

3.1 3D active contour algorithm

Active contour models are based on a curve (i.e. contour in 2D or surface in 3D) that evolves following different constraints given by the image. Traditionally, evolving constraints are based on the gradient of the image (Kass et al., 1987; Caselles et al., 1997), being suitable only for images with edges well defined by gradients. However, in 3D CT abdominal images, liver boundaries are not completely defined by a gradient. As we can observe in Fig. 1 the proximity of the liver to other organs of similar CT intensity values prevents from defining all the edges using only gradient information.

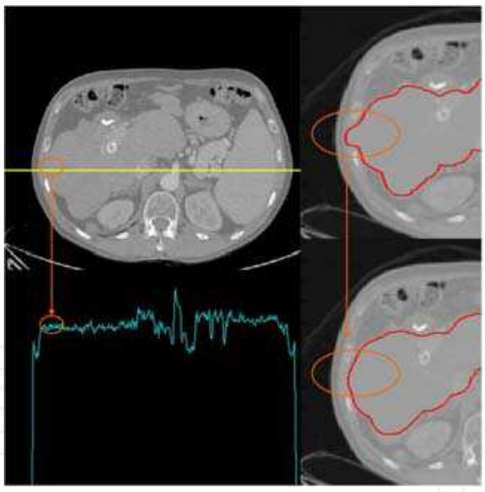

Fig. 1. *On the left*: transverse slice of an abdominal CT image and its profile of intensities along the yellow line showing the difficulty of establishing an intensity threshold between liver and adjacent intercostal muscles. *On the right*: active contour growing based on a classical gradient dependent definition *(above)* and the improvement introduced by the proposed method that avoids the contour to overflow among the intercostal space *(below)*.

In order to segment objects with boundaries not necessarily defined by a gradient, (Chan & Vese, 2001) proposed an active contour method consisting on the minimization of a force that depends on the image gray values inside and outside the curve at each iterative step. This method is based on Mumford-Shah segmentation techniques (Mumford & Shah, 1989):

$$F = \lambda_1 \int_{inside(C)} \left|u_0(x,y) - c_1\right|^2 dxdy + \lambda_2 \int_{outside(C)} \left|u_0(x,y) - c_2\right|^2 dxdy \quad (1)$$

where u_0 is a given image formed by two regions, C is an evolving contour, and the constants c_1 and c_2 are the averages of u_0 inside and outside C respectively.
This force can be formulated by Level Sets techniques as described in (Chan & Vese, 2001). Level Sets based active contour implementations have become very popular, due to their ability of handling discontinuities and the possibility of topological changes. For the Level Sets formulation, C is represented by a Lipschitz function ϕ:

$$\begin{aligned} C &= \partial\omega\{(x,y) \in \Omega : \phi(x,y) = 0\} \\ inside(C) &= \omega = \{(x,y) \in \Omega : \phi(x,y) < 0\} \\ outside(C) &= \Omega / \bar{\omega} = \{(x,y) \in \Omega : \phi(x,y) > 0\} \end{aligned} \quad (2)$$

The function (1) can be expressed using ϕ and the Heaviside H and Dirac δ_0 functions. The associated Euler–Lagrange equation for ϕ is deduced by minimizing the function with respect to ϕ. Finally, a linear system is obtained that can be solved by an iterative method (for more details we refer the reader to (Chan & Vese, 2001)):

$$\begin{aligned} \frac{\phi_{i,j}^{n+1} - \phi_{i,j}^{n}}{\Delta t} = \delta_h(\phi_{i,j}^{n}) \Bigg[\mu \cdot div\left(\frac{\nabla\phi^n}{\left|\nabla\phi^n\right|}\right) - \gamma \\ + \lambda_1 (u_{0,i,j} - c_1(\phi^n))^2 - \lambda_2 (u_{0,i,j} - c_2(\phi^n))^2 \Bigg] \end{aligned} \quad (3)$$

where $\mu \geq 0$, $\gamma \geq 0$, $\lambda 1$, $\lambda 2 > 0$ are fixed parameters and Δt and h are the time and space steps respectively, used to discretize the equation in ϕ with a finite difference implicit scheme. The term $div(\nabla\phi^n / |\nabla\phi^n|)$ is used to restrict the curvature of the contour. Subscripts i, j represent the position.
With parameters $\lambda 1 = \lambda 2 = 1$ the equation produces a lineal force that is annulled in the mean value of intensity averages $c1$ and $c2$ .With this definition the contour stops only when there is a notable difference between clear zones toward darker zones and not with sudden zones of very extreme intensities; so this method works properly only with those images that contain two homogenously well defined regions and textures. If there is a small area with an extreme intensity closer to $c1$ than to $c2$, it will be erroneously included into the segmentation, even when differing to $c1$ more than the absolute difference between $c1$ and $c2$. An example of this problem, hardly controlled by modifying $\lambda 1$ and $\lambda 2$ weights, can be appreciated in Fig. 2 (left) showing a contour based on the (Chan & Vese, 2001) equation growing into the ribs.
In order to solve this problem, some variations inside the function defined in (Chan & Vese, 2001) are proposed in (Fernandez-de-Manuel et al., 2009) to allow segmenting a homogenous region (liver) that is adjacent to other organs with higher or lower intensities in hepatic CT scans with a variable anatomy complexity. The proposed active contour method restricts the growth of the contour to a zone limited around the average gray value inside the liver. It combines both the modified energy function based on gray values, and a morphological gradient information in order to make the algorithm more robust. The Level Sets function derives from equation (1) and considerably improves the segmentation results on the hepatic images under study. The resulting linear system proposed in (Fernandez-de-Manuel et al., 2009), solved by iterative methods, is the following:

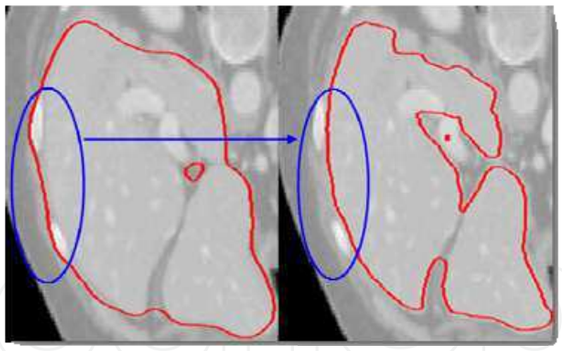

Fig. 2. *On the left*: 3D Active contour growing based on (Chan & Vese, 2001). *On the right*: 3D Active contour growing based on the redefinition of the force equation proposed in (Fernandez-de-Manuel et al., 2009). The growing of the contour into the ribs is successfully controlled in the right image.

$$\frac{\phi_{i,j,k}^{n+1}-\phi_{i,j,k}^{n}}{\Delta t}=\delta_h(\phi_{i,j,k}^{n})\left[\mu\cdot div\left(\frac{\nabla\phi^{n}}{|\nabla\phi^{n}|}\right)-\gamma\right.$$
$$\left.+\lambda_1\left|u_{0,i,j,k}-\rho\nabla u_{0,i,j,k}-c_1(\phi^{n})\right|-\lambda_2\left|c_1(\phi^{n})-c_2(\phi^{n})\right|\right] \quad (4)$$

where u_0 is a 3D image formed by two regions, one with almost constant intensity (liver), and the other one with different intensity organs. ϕ represents the evolving 3D contour. $\mu\geq 0$, $\gamma\geq 0$, ρ, $\lambda 1$, $\lambda 2>0$ are fixed parameters, the constants c_1 and c_2 depending on iteration n are the averages of u_0 inside and outside the contour respectively and Δt and h are the time and space steps respectively. The term $div(\nabla\phi^n/|\nabla\phi^n|)$ is used to restrict the curvature of the 3D contour. Subscripts i, j, k represent the position in the image. The algorithm starts with a small surface obtained from a seed point placed inside the healthy liver. The initial surface grows iteratively following the described linear system (4). The method has been implemented for 3D images inside a MATLAB framework limiting the force evaluation to a narrow band around the contour in order to reduce the complexity.

3.2 3D Multi-resolution strategy

Due to the large size of CT abdominal images, the method has been implemented following a multiresolution strategy in order to reduce computation time. Three pyramidal steps have been used (Fig. 3). In the first step, the resolution of the images is reduced by a factor of 4. This fast initial segmentation allows us to select the liver region and to get a first approximate surface. In the second step, the resolution is reduced by a factor of 2. A bicubic interpolation is applied in the resolution reduction process. At each step the growing surface begins with the previous step result and iterates to the actual surface of the liver. Finally, in the last step, the resolution of the image is the original one and it performs a final growing of the previous surface that segments properly the liver.

3.3 Pre-processing and definition of frontiers

The general active contour method is extended with a pre-processing step to address particular problems.

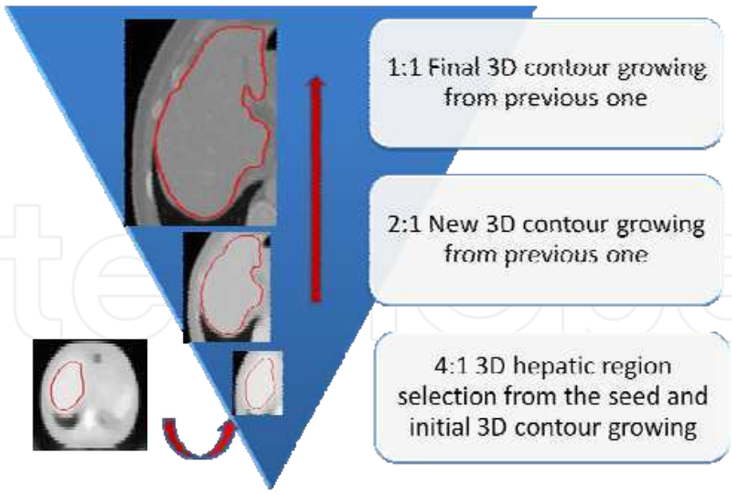

Fig. 3. Diagram of proposed pyramidal segmentation steps.

Firstly, in order to guarantee that the surface evolution properties are properly fitted to the data, an interpolation is applied to make images isotropic. Next, a median filter eliminates inhomogeneities inside the liver region. Kernel size is 3 in lowest resolution levels and no median filter is used in the higher resolution level.
In order to define 3D frontiers with conflictive regions, 6 points (3 segments) are selected. Each one of the segments is manually defined in each dimension (transverse, coronal and sagittal) using a multiplanar 3D viewer. These segments are integrated to reconstruct a parallelogram in the 3D space that approximates the restricted plane that separates the liver from the conflictive region. This approach allows the user to define 3D frontiers with minimal interaction. Then, a modification of the image gray values with an exponential function that grows from zero to the original gray image value around the 3D frontier is incorporated in order to restrict the surface growing around the selected area. Frontiers are typically needed for the cava vein, heart or kidney.

3.4 Post-processing

The active contour functional has been chosen carefully and its operation is convenient. However, a post-processing step is always essential in any kind of tool in order to smooth the results and fill-in small gaps. In the presented work, resulting segmentations are automatically refined with additional post-processing in order to recover original spatial representation, to smooth the surface and to eliminate unconnected zones. To complete this last step, a morphological erosion is applied to the resulting segmentation mask followed by a binary morphological reconstruction of the mask from the original seed point and a final morphological dilation.

4. Data and validation

The presented liver segmentation tool has been validated on five abdominal CT examinations (Table 1). The set includes cases of different liver size, shape, intensity and pathologic state. Studies 1, 2, 4 and 5 were acquired on a Philips Brilliance 16 slice CT

scanner, and study 3 was acquired on a Philips AV Expander spiral CT. The pixel spacing varied between 0.69 and 0.84 mm, the inter-slice distance varied from 1 to 5 mm.
The images were segmented manually by radiologists, working slice-by-slice in transverse view. These manual segmentations were performed using all the slices of the study. The liver region was defined as the entire healthy parenchyma, excluding tumors and lesions in order to avoid overestimating the liver functional volume.
The semiautomatic segmentation has been carried out following steps described in Section 3. The Level-Sets function parameters (4) were fixed to γ=0, ρ=1, $\lambda 1$=1 and $\lambda 2$= 1/5.5 as these values were presented in (Fernandez-de-Manuel et al., 2009) as the ones with better results in CT scans.
The obtained segmentations have been evaluated by five metrics based on the ones described on (Heimann et al., 2009). This five metrics are as follows:

Volumetric Overlap Error (VOE), in percent:

$$VOE = \left(1 - \left(N_i \,/\, N_u\right)\right) \cdot 100 \tag{5}$$

where N_i is the number of voxels in the intersection of resulting segmentation and reference, and N_u is the number of voxels in the union of resulting segmentation and reference. This value is 0 for a perfect segmentation and 100 when there is no overlap.

Relative Volume Difference (RVD), in percent:

$$RVD = \left((V_s - V_r) \,/\, V_r\right) \cdot 100 \tag{6}$$

where V_s is the volume of the segmentation, and V_r is the volume of the reference. The best value is 0 (for exact volumes) and the worst one is 100.

Average Symmetric Surface Distance (ASSD), in mm:

$$d_i = dist(B_{s,i}, B_{r,i}),\ \forall i \quad \text{ASSD} = mean(d_i) \tag{7}$$

where $B_{s,i}$ is the edge voxel i of one of the images, and $B_{r,i}$ is the edge voxel i of the other (the closest voxel to $B_{s,i}$). Border voxels are those belonging to the segmented liver that have at least one of their 18 nearest neighbors not belonging to the segmented liver. *dist* represents the Euclidean distance, not signed, in mm and taking into account the different resolutions in the different scan directions. Distances between the two sets of border voxels (one set from each image) are stored. *mean* represents the mean value of distances. ASSD value is 0 for a perfect segmentation.

Root Mean Square Symmetric Surface Distance (RMSD), in mm:

$$d_i = dist(B_{s,i}, B_{r,i}),\ \forall i \quad RMSD = \sqrt{mean\left(\left(d_i\right)^2\right)} \tag{8}$$

This measure is similar to the previous one but in this case the squared distances between the two sets of border voxels are stored. RMSD value is 0 for a perfect segmentation.

Maximum Symmetric Surface Distance (MSSD), in mm:

$$d_i = dist(B_{s,i}, B_{r,i}),\ \forall i \quad \text{MSSD} = \max(d_i) \tag{9}$$

This measure is similar to the previous two, but in this case the maximum of all distance is taken instead of the average. MSSD is 0 for a perfect segmentation.

5. Results and discussion

Table 1 shows the experiment results including case descriptions, the number of required frontiers manually selected by the user, resulting metrics, and the computation time for each examination.

We can see that volume differences (absolute values of RVD) are smaller than 10% in all of the cases (Table 1). In all of them, the deviation is produced because of under-segmentation. Analyzing in detail the resulting images, we conclude that the region affected by these under-segmentations is, in the majority of the cases, the narrow end of the left liver lobe. This problem affects specially to the case 1 and the case 5, producing a Maximum Surface Distance bigger than 3 cm, which is exactly located in those narrow areas. Case 1 is probably the most difficult case presenting a very atypical shape and gray level distribution. In these narrow regions, the 3D contour finds difficulties to grow due to particularly restrictive curvature constraints. Further studies are warranted to correct the small misclassified areas by modifying curvature restrictions locally.

Most of the tumors were not included in the liver region, according to the requirements of the clinicians. In this sense, the proposed method works properly, as it excludes hyperintense and hypointense large tumors (Fig. 4). However, in some of the cases, small metastases completely surrounded by healthy parenchyma were not excluded during the process of contour growing, affecting considerable to the Surface Distance Errors (case 3). Nevertheless, this problem hardly modifies the final volume estimation, because of its small size.

Other segmentation minor errors were detected in the surroundings of the hepatic portal vein (case 2 and 4).

Case	Case description	# frontiers	VOE [%]	RVD [%]	ASSD [mm.]	RMSD [mm.]	MSSD [mm.]	Time [min.]
1	Hepatic carcinoma	13	13.13	-9.02	2.39	5.12	42.84	9.57
2	Liver after hepatectomy	0	10.80	-5.76	1.43	2.04	14.25	9.92
3	Portal embolization pre- right hepatectomy	4	10.48	-6.38	1.24	2.72	27.04	11.56
4	Metastasis	2	11.55	-4.46	1.79	3.09	21.91	3.67
5	Portal embolization pre- right hepatectomy	0	13.04	-9.41	2.13	3.67	33.44	3.82

Table 1. Cases descriptions, number of initial frontiers points, resulting metrics and computation times.

In general, resulting segmentations satisfied clinical requirements. Overlap errors, and volume errors were considered reasonable. Special attention will be made in further studies in order to solve problems affecting small areas. However, although Maximum Distance Errors (MSSD) were considerably high, the reasonable averages (ASSD and RMSD) show that these errors were produced in very punctual areas hardly modifying volumes. Most of the frontiers were defined in zones adjacent to the heart and cava vein. The number of frontiers needed to restrict forces in those areas depended on the image and varied from 0 to 13 frontiers in the most difficult case. Further studies are also warranted in order to reduce the user interaction.

The proposed method requires 7.7 minutes on average using a non optimized MATLAB code running on one core of a PC at 2.4 GHz with 4 GB memory.

Time refers to the time needed for the automated computation of the segmentation result after the seed point and frontiers have been set. Computation time depends on the image size, mainly on the inter-slice distance (that vary from 1 to 5 mm in our data) and this is the reason because it goes from 3 to 11 min. Note that the highest resolution level of the process employ all the slices of the original data and this is the more time-consuming step.

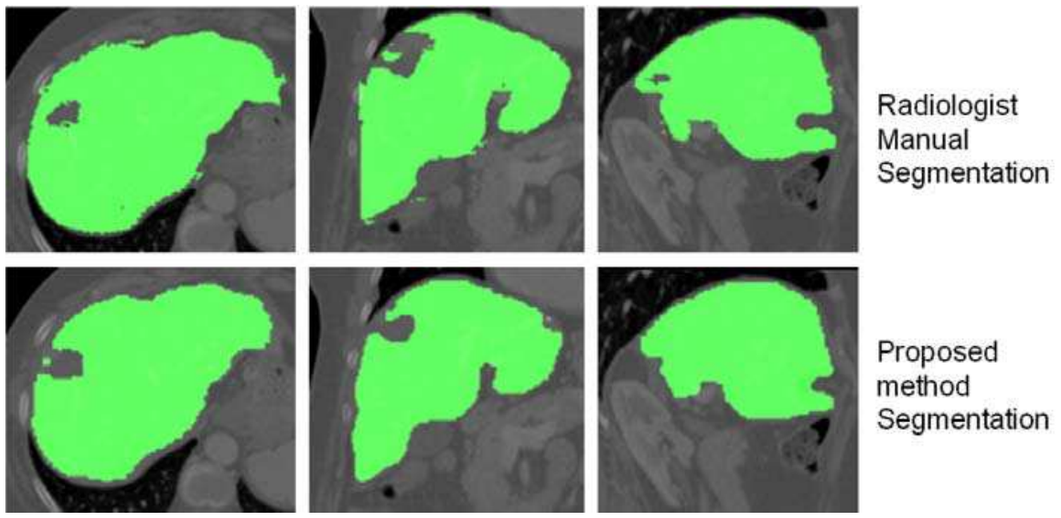

Fig. 4. Segmentation of healthy parenchyma in case 4. *Top*: radiologist manual segmentation. *Bottom*: resulting semiautomatic segmentation with presented method. Left to right: transverse, coronal and sagittal slices.

6. Conclusion

This chapter makes an especial effort in presenting, in a wide and complete context, the state of the art in the scope of the hepatic segmentation from CT images. It presents the newest and most sophisticated methods developed in this field in the last few years and notes the importance of hepatic volume estimation from CT scans for hepatic surgical planning. Moreover, the application of a semiautomatic liver 3D segmentation tool to segment and quantify the volume of the healthy parenchyma from CT preoperative abdominal images is presented. The tool combines a 3D active contour method implemented with Level Sets techniques with a multiresolution strategy, a morphological filtering post processing and a fast method to manually define specific frontiers. An initial seed point inside the healthy

parenchyma manually selected by the user is required. If desired the user can also define several frontiers to delineate the separation with problematic regions like the kidney or the heart. The method has been validated with a set of five abdominal CT preoperative images with special difficulties. Further studies are needed in order to solve specific problems related with errors in narrow liver areas and reducing user interaction. Nevertheless, the proposed method has demonstrated good performance and a noticeable reduction of the time needed with respect to manual segmentations.

7. Acknowledgments

This study was partially supported by research projects TIN 2007-68048-C02, PI09/91058, PI09/91065, ENTEPRASE PS-300000-2009-5, AMIT-CDTI, TEC2010-21619-C04 and PRECISION IPT-300000-2010-3, from Spain's Ministry of Science & Innovation, the project ARTEMIS Comunidad de Madrid, and with assistance from the European Regional Development Fund (FEDER).

8. References

Barrett, W. A. & Mortensen, E. N. (1997). Interactive live-wire boundary extraction. *Med Image Anal,* Vol. 1, No. 4, pp. 331-41.

Beck, A. & Aurich, V. (2007). HepaTux–A Semiautomatic Liver Segmentation System. *Proceedings of MICCAI 2007 Workshop: 3D Segmentation in the Clinic-A Grand Challenge,* pp. 225–233.

Beichel, R.; Bauer, C.; Bornik, A.; Sorantin, E. & Bischof, H. (2007). Liver Segmentation in CT Data: A Segmentation Refinement Approach. *Proceedings of MICCAI 2007 Workshop: 3D Segmentation in the Clinic-A Grand Challenge,* pp. 235–245.

Bekes, G.; Nyül, L. G.; Máté, E.; Kuba, A. & M., F. (2007). 3D Segmentation of Liver, Kidneys and Spleen from CT Images. *International Journal of Computer Assisted Radiology and Surgery,* Vol. 2, pp. 45-46.

Campadelli, P.; Casiraghi, E. & Pratissoli, S. (2010). A segmentation framework for abdominal organs from CT scans. *Artif Intell Med,* Vol. 50, No. 1, pp. 3-11.

Caselles, V.; Kimmel, R. & Sapiro, G. (1997). Geodesic active contours. *International Journal of Computer Vision,* Vol. 22, No. 1, pp. 61-79.

Couinaud, C. (1999). Liver anatomy: portal (and suprahepatic) or biliary segmentation. *Digestive Surgery,* Vol. 16, No. 6, pp. 459-467.

Chan, T. F. & Vese, L. A. (2001). Active contours without edges. *IEEE Transactions on Image Processing,* Vol. 10, No. 2, pp. 266-277.

Dawant, B. M.; Li, R.; Lennon, B. & Li, S. (2007). Semi-automatic segmentation of the liver and its evaluation on the MICCAI 2007 grand challenge data set. *Proceedings of MICCAI 2007 Workshop: 3D Segmentation in the Clinic-A Grand Challenge,* pp. 215–221.

Fernandez-De-Manuel, L.; Rubio, J. L.; Ledesma-Carbayo, M. J.; Pascau, J.; Tellado, J. M.; Ramón, E.; Desco, M. & Santos, A. (2009). 3D Liver Segmentation in Preoperative CT Images using a Level-Sets Active Surface Method. *Proceedings of IEEE Engineering in Medicine and Biology Society (EMBC 2009),* pp. 3625-3628.

Fujimoto, H.; Gu, L. & Kaneko, T. (2002). Recognition of abdominal organs using 3D mathematical morphology. *Systems and Computers in Japan,* Vol. 33, No. 8, pp. 75-83.

Gao, L. M.; Heath, D. G. & Fishman, E. K. (1998). Abdominal image segmentation using three-dimensional deformable models. *Investigative Radiology,* Vol. 33, No. 6, pp. 348-355.

Gao, L. M.; Heath, D. G.; Kuszyk, B. S. & Fishman, E. K. (1996). Automatic liver segmentation technique for three-dimensional visualisation of CT data. *Radiology,* Vol. 201, No. 2, pp. 359-364.

Garamendi, J. F.; Malpica, N.; Martel, J. & Schiavi, E. (2007). Automatic segmentation of the liver in CT using level sets without edges. *Proceedings of Iberian Conference on Pattern Recognition and Image Analysis,* pp. 161-168.

Handels, H. & Ehrhardt, J. (2009). Medical Image Computing for Computer-supported Diagnostics and Therapy Advances and Perspectives. *Methods of Information in Medicine,* Vol. 48, No. 1, pp. 11-17.

Heimann, T.; Meinzer, H. P. & Wolf, I. (2007). A statistical deformable model for the segmentation of liver CT volumes. *Proceedings of MICCAI 2007 Workshop: 3D Segmentation in the Clinic-A Grand Challenge,* pp. 161–166.

Heimann, T.; Van Ginneken, B.; Styner, M. A.; Arzhaeva, Y.; Aurich, V.; Bauer, C.; Beck, A.; Becker, C.; Beichel, R.; Bekes, G.; Bello, F.; Binnig, G.; Bischof, H.; Bornik, A.; Cashman, P. M. M.; Chi, Y.; Cordova, A.; Dawant, B. M.; Fidrich, M.; Furst, J. D.; Furukawa, D.; Grenacher, L.; Hornegger, J.; Kainmuller, D.; Kitney, R. I.; Kobatake, H.; Lamecker, H.; Lange, T.; Lee, J.; Lennon, B.; Li, R.; Li, S.; Meinzer, H. P.; Nemeth, G.; Raicu, D. S.; Rau, A. M.; Van Rikxoort, E. M.; Rousson, M.; Rusko, L.; Saddi, K. A.; Schmidt, G.; Seghers, D.; Shimizu, A.; Slagmolen, P.; Sorantin, E.; Soza, G.; Susomboon, R.; Waite, J. M.; Wimmer, A. & Wolf, I. (2009). Comparison and Evaluation of Methods for Liver Segmentation From CT Datasets. *IEEE Transactions on Medical Imaging,* Vol. 28, No. 8, pp. 1251-1265.

Jiang, H. Y. & Cheng, Q. S. (2009) Automatic 3D Segmentation of CT Images Based on Active Contour Models. IN Thalmann, D.;Shah, J. J. & Peng, Q. S. (Eds.) *2009 11th IEEE International Conference on Computer-Aided Design and Computer Graphics, Proceedings.* pp. 540-543.

Kainmueller, D.; Lange, T. & Lamecker, H. (2007). Shape constrained automatic segmentation of the liver based on a heuristic intensity model. *Proceedings of MICCAI 2007 Workshop: 3D Segmentation in the Clinic-A Grand Challenge,* pp. 109-116.

Kass, M.; Witkin, A. & Terzopoulos, D. (1987). Snakes-Active Contour Models. *International Journal of Computer Vision,* Vol. 1, No. 4, pp. 321-331.

Koss, J. E.; Newman, F. D.; Johnson, T. K. & Kirch, D. L. (1999). Abdominal organ segmentation using texture transforms and a Hopfield neural network. *IEEE Transactions on Medical Imaging,* Vol. 18, No. 7, pp. 640-648.

Lamecker, H.; Lange, T. & Seebass, M. (2004) Segmentation of the liver using a 3d statistical shape model. *Technical report, Zuse Institute Berlin.*

Lee, C. C. & Chung, P. C. (2000). Recognizing abdominal organs in CT images using contextual neural network and fuzzy rules. *Proceedings of 22nd Annual International Conference of the IEEE Engineering in Medicine and Biology Society,* pp. 1745-1748.

Lee, C. C.; Chung, P. C. & Tsai, H. M. (2003). Identifying multiple abdominal organs from CT image series using a multimodule contextual neural network and spatial fuzzy rules. *IEEE Transactions on Information Technology in Biomedicine,* Vol. 7, No. 3, pp. 208-217.

Lee, J.; Kim, N.; Lee, H.; Seo, J. B.; Won, H. J.; Shin, Y. M. & Shin, Y. G. (2007). Efficient liver segmentation exploiting level-set speed images with 2.5 D shape propagation. *Proceedings of MICCAI 2007 Workshop: 3D Segmentation in the Clinic-A Grand Challenge,* pp. 189–196.

Lim, S. J.; Jeong, Y. Y. & Ho, Y. S. (2005). Segmentation of the liver using the deformable contour method on CT images. *Proceedings of SPIE,* pp. 570-581.

Lim, S. J.; Jeong, Y. Y. & Ho, Y. S. (2006). Automatic liver segmentation for volume measurement in CT images. *Journal of Visual Communication and Image Representation,* Vol. 17, No. 4, pp. 860-875.

Lim, S. J.; Jeong, Y. Y.; Lee, C. W. & Ho, Y. S. (2004). Automatic segmentation of the liver in CT images using the watershed algorithm based on morphological filtering. *Proceedings of SPIE,* pp. 1658.

Linguraru, M. G.; Sandberg, J. K.; Li, Z. X.; Shah, F. & Summers, R. M. (2010). Automated segmentation and quantification of liver and spleen from CT images using normalized probabilistic atlases and enhancement estimation. *Medical Physics,* Vol. 37, No. 2, pp. 771-783.

Liu, F.; Zhao, B. S.; Kijewski, P. K.; Wang, L. & Schwartz, L. H. (2005). Liver segmentation for CT images using GVF snake. *Medical Physics,* Vol. 32, No. 12, pp. 3699-3706.

Luo, S. H.; Hu, Q. M.; He, X. J.; Li, J. M.; Jin, J. S. & Park, M. (2009). Automatic Liver Parenchyma Segmentation from Abdominal CT Images Using Support Vector Machines. *Proceedings of 2009 Icme International Conference on Complex Medical Engineering,* pp. 522-526.

Montagnat, J. & Delingette, H. (1997). Volumetric medical images segmentation using shape constrained deformable models. *Proceedings of First Joint Conference CVRMED-MRCAS'97,* pp. 13-22.

Mumford, D. & Shah, J. (1989). Optimal approximations by piecewise smooth functions and associated variational problems. *Comm. Pure Appl. Math,* Vol. 42, No. 5, pp. 577-685.

Pan, S. Y. & Dawant, B. M. (2001). Automatic 3D segmentation of the liver from abdominal CT images: a level-set approach. *Medical Imaging: 2001: Image Processing, Pts 1-3,* Vol. 2, No. 27, pp. 128-138.

Park, H.; Bland, P. H. & Meyer, C. R. (2003). Construction of an abdominal Probabilistic atlas and its application in segmentation. *IEEE Transactions on Medical Imaging,* Vol. 22, No. 4, pp. 483-492.

Platero, C.; Poncela, J. M.; Gonzalez, P.; Tobar, M. C.; Sanguino, J.; Asensio, G. & Santos, E. (2008). Liver segmentation for hepatic lesions detection and characterisation. *Proceedings of IEEE International Symposium on Biomedical Imaging: from Nano to Macro*, pp. 13-16.

Pohle, R. & Toennies, K. D. (2001). Segmentation of medical images using adaptive region growing. *Medical Imaging: 2001: Image Processing, Pts 1-3,* Vol. 2, No. 27, pp. 1337-1346.

Radtke, A.; Nadalin, S.; Sotiropoulos, G. C.; Molmenti, E. P.; Schroeder, T.; Valentin-Gamazo, C.; Lang, H.; Bockhorn, M.; Peitgen, H. O.; Broelsch, C. E. & Malago, M. (2007). Computer-assisted operative planning in adult living donor liver transplantation: A new way to resolve the dilemma of the middle hepatic vein. *World Journal of Surgery,* Vol. 31, No. 1, pp. 175-185.

Ruskó, L.; Bekes, G.; Németh, G. & M., F. (2007). Fully Automatic Liver Segmentation for Contrast-enhanced CT Images. . *Proceedings of MICCAI 2007 Workshop: 3D Segmentation in the Clinic-A Grand Challenge,* pp. 143-150.

Ryu, M. & Cho, A. (Eds.) (2009) *The New Liver Anatomy: Portal Segmentation and the Drainage Vein,* Springer, ISBN 978-4-431-95992-2, New York.

Saddi, K.; Rousson, M.; Chefd'hotel, C. & Cheriet, F. (2007). Global-to-Local Shape Matching for Liver Segmentation in CT Imaging. *Proceedings of MICCAI 2007 Workshop: 3D Segmentation in the Clinic-A Grand Challenge,* pp. 207-214.

Schenk, A.; Prause, G. & Peitgen, H. O. (2000). Efficient semiautomatic segmentation of 3D objects in medical images. *Proceedings of Medical Image Computing and Computer-Assisted Intervention - MICCAI 2000,* pp. 186-195.

Schenk, A.; Prause, G. & Peitgen, H. O. (2001). Local cost computation for efficient segmentation of 3D objects with live wire. *Medical Imaging: 2001: Image Processing, Pts 1-3,* Vol. 2, No. 27, pp. 1357-1364.

Shimizu, A.; Ohno, R.; Ikegami, T.; Kobatake, H.; Nawano, S. & Smutek, D. (2006). Multi-organ segmentation in three dimensional abdominal CT images. *International Journal of Computer Assisted Radiology and Surgery (CARS 2006)* Vol. 1, No. 7, pp. 76-78.

Soler, L.; Delingette, H.; Malandain, G.; Montagnat, J.; Ayache, N.; Koehl, C.; Dourthe, O.; Malassagne, B.; Smith, M.; Mutter, D. & Marescaux, J. (2001). Fully automatic anatomical, pathological, and functional segmentation from CT scans for hepatic surgery. *Comput Aided Surg,* Vol. 6, No. 3, pp. 131-42.

Suzuki, K.; Kohlbrenner, R.; Epstein, M. L.; Obajuluwa, A. M.; Xu, J. W. & Hori, M. (2010). Computer-aided measurement of liver volumes in CT by means of geodesic active contour segmentation coupled with level-set algorithms. *Medical Physics,* Vol. 37, No. 5, pp. 2159-2166.

Tsai, D. Y. & Tanahashi, N. (1994). Neural-Network-Based Boundary Detection of Liver Structure in Ct Images for 3-D Visualization. *1994 Ieee International Conference on Neural Networks, Vol 1-7,* Vol., 3484-3489.

Van Ginneken, B.; Heimann, T. & Styner, M. (2007). 3D segmentation in the clinic: A grand challenge. *Proceedings of MICCAI 2007 Workshop: 3D Segmentation in the Clinic-A Grand Challenge,* pp. 7.

Wimmer, A.; Soza, G. & Hornegger, J. (2007). Two-stage semi-automatic organ segmentation framework using radial basis functions and level sets. *Proceedings of MICCAI 2007 Workshop: 3D Segmentation in the Clinic-A Grand Challenge,* pp. 179–188.

Woodhouse, C. E.; Ney, D. R.; Sitzmann, J. V. & Fishman, E. K. (1994). Spiral Computed-Tomography Arterial Portography with 3-Dimensional Volumetric Rendering for Oncologic Surgery Planning - a Retrospective Analysis. *Investigative Radiology,* Vol. 29, No. 12, pp. 1031-1037.

Zhou, X.; Kitagawa, T.; Okuo, K.; Hara, T.; Fujita, H.; Yokoyam, R.; Kanematsu, M. & Hoshi, H. (2005). Construction of a probabilistic atlas for automated liver segmentation in non-contrast torso CT images. *Proceedings of CARS 2005: Computer Assisted Radiology and Surgery,* pp. 1169-1174.

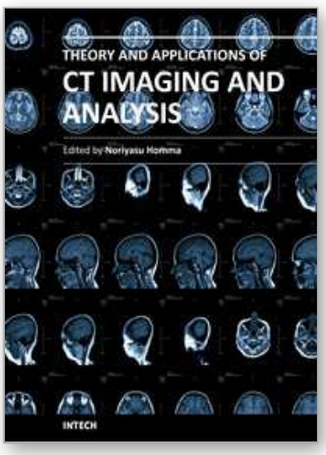

Theory and Applications of CT Imaging and Analysis
Edited by Prof. Noriyasu Homma

ISBN 978-953-307-234-0
Hard cover, 290 pages
Publisher InTech
Published online 04, April, 2011
Published in print edition April, 2011

The x-ray computed tomography (CT) is well known as a useful imaging method and thus CT images have continuingly been used for many applications, especially in medical fields. This book discloses recent advances and new ideas in theories and applications for CT imaging and its analysis. The 16 chapters selected in this book cover not only the major topics of CT imaging and analysis in medical fields, but also some advanced applications for forensic and industrial purposes. These chapters propose state-of-the-art approaches and cutting-edge research results.

How to reference
In order to correctly reference this scholarly work, feel free to copy and paste the following:

Laura Fernandez-de-Manuel, Maria J. Ledesma-Carbayo, Daniel Jimenez-Carretero, Javier Pascau, Jose L. Rubio-Guivernau, Jose M. Tellado, Enrique Ramon, Manuel Desco and Andres Santos (2011). Liver Segmentation and Volume Estimation from Preoperative CT Images in Hepatic Surgical Planning: Application of a Semiautomatic Method Based on 3D Level Sets, Theory and Applications of CT Imaging and Analysis, Prof. Noriyasu Homma (Ed.), ISBN: 978-953-307-234-0, InTech, Available from: http://www.intechopen.com/books/theory-and-applications-of-ct-imaging-and-analysis/liver-segmentation-and-volume-estimation-from-preoperative-ct-images-in-hepatic-surgical-planning-ap

INTECH
open science | open minds

InTech Europe
University Campus STeP Ri
Slavka Krautzeka 83/A
51000 Rijeka, Croatia
Phone: +385 (51) 770 447
Fax: +385 (51) 686 166
www.intechopen.com

InTech China
Unit 405, Office Block, Hotel Equatorial Shanghai
No.65, Yan An Road (West), Shanghai, 200040, China
中国上海市延安西路65号上海国际贵都大饭店办公楼405单元
Phone: +86-21-62489820
Fax: +86-21-62489821

IntechOpen